Capacitance and Effective Area of Flush Monopole Probes

Larry K. Warne, Lorena I. Basilio, William A. Johnson, Marvin E. Morris
Electromagnetics and Plasma Physics Analysis Dept.

Matthew B. Higgins
Applied Accelerator and Electromagnetic Technology Dept.

Jane M. Lehr
Advanced Pulsed Power Technologies Dept.

Sandia National Laboratories
P. O. Box 5800
Albuquerque, NM 87185-1152

Abstract

Approximate formulas are constructed and numerical simulations are carried out for electric field derivative probes that have the form of flush mounted monopoles. Effects such as rounded edges are included. A method is introduced to make results from two-dimensional conformal mapping analyses accurately apply to the three-dimensional axisymmetric probe geometry.

Intentionally Left Blank

Contents

Figures

Figure 1. Probe geometry.

1 INTRODUCTION

This report estimates the capacitance and effective area of an electric field derivative probe. The probe is a transmission line terminating in a flush mounted monopole antenna as depicted in Figure 1. (Previous studies on coaxially-driven antennas include [1], [2], and [3].) For the flush mounted probe analyzed in this study, the outer and inner radii are

$$b \approx 0.189 \text{ in}$$

$$a \approx 0.121 \text{ in}$$

.

2 WATER PERMITTIVITY

Water is often used as the dielectric material. The permittivity is found from [4]

$$\varepsilon/\varepsilon_0 \approx 88.15 - 41.4\theta + 13.1\theta^2 - 4.6\theta^3$$

for $0^o\text{C} < T < 60^o\text{C}$, where

$$\theta = T/\left(100^o \text{ C}\right)$$
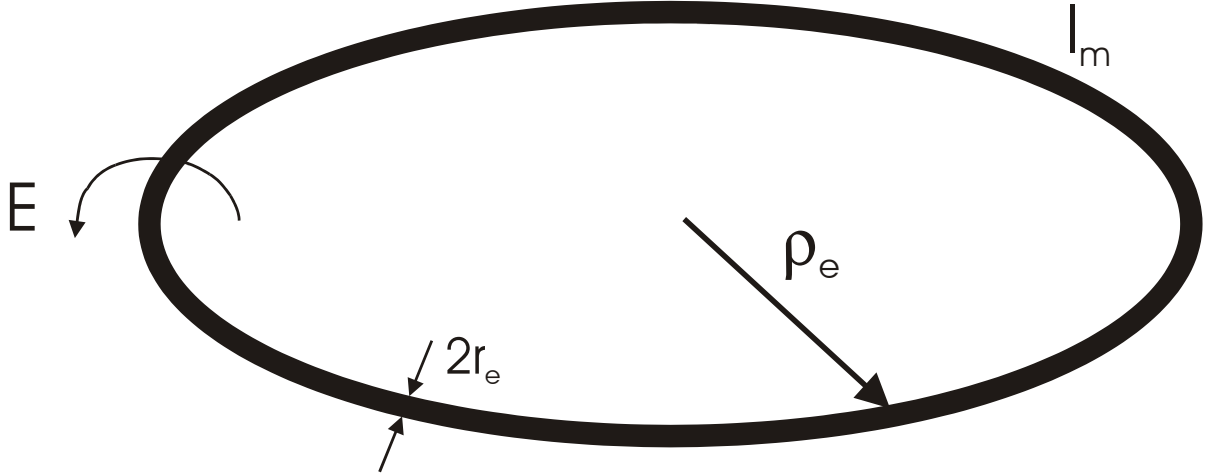
Figure 2. Antenna gap is modeled as a magnetic current loop.

$$\varepsilon_0 \approx 8.854 \text{ pF/m}$$

is the permittivity of free space. At $T = 20°C$ we find $\varepsilon/\varepsilon_0 \approx 80.4$. For pure water this value is nearly frequency independent up to about 1 GHz [4].

3 MAGNETIC CURRENT LOOP

The antenna gap is modeled in this section as a loop of magnetic current as shown in Figure 2.

The electric field is related to the magnetic current by means of

$$\nabla \times \underline{E} = -\underline{J}_m$$

The electric vector potential is introduced by means of

$$\underline{D} = \varepsilon\underline{E} = -\nabla \times \underline{A}_e$$

Taking the electric vector potential to be divergence free, we obtain

$$-\nabla \times \nabla \times \underline{A}_e = \nabla^2\underline{A}_e = -\varepsilon\underline{J}_m$$

Therefore using the free space static Green's function, the solution is

$$\underline{A}_e\left(\underline{r}\right) = \frac{\varepsilon}{4\pi}\int_V \underline{J}_m\left(\underline{r}'\right)\frac{dV'}{|\underline{r}-\underline{r}'|}$$

The electric vector potential of a loop of magnetic current

$$J_{m\varphi} = I_m\delta\left(z\right)\delta\left(\rho - \rho_e\right)$$

with radius ρ_e is φ-directed and given by

$$A_{e\varphi} = \frac{\varepsilon I_m}{4\pi} \rho_e \int_\varphi^{2\pi+\varphi} \frac{\cos(\varphi - \varphi')\, d\varphi'}{\sqrt{z^2 + \rho^2 + \rho_e^2 - 2\rho\rho_e \cos(\varphi - \varphi')}}$$

$$= \frac{\varepsilon I_m}{4\pi(2\rho)} \int_{-\pi}^{\pi} \frac{\left[(z^2 + \rho^2 + \rho_e^2) - (z^2 + \rho^2 + \rho_e^2) - 2\rho\rho_e \cos\varphi'\right] d\varphi'}{\sqrt{z^2 + \rho^2 + \rho_e^2 + 2\rho\rho_e \cos\varphi'}}$$

$$= \frac{\varepsilon I_m}{4\pi\rho} \int_0^{\pi} \left[\frac{(z^2 + \rho^2 + \rho_e^2)}{\sqrt{z^2 + \rho^2 + \rho_e^2 + 2\rho\rho_e \cos\varphi'}} - \sqrt{z^2 + \rho^2 + \rho_e^2 + 2\rho\rho_e \cos\varphi'} \right] d\varphi'$$

Letting

$$\sqrt{z^2 + \rho^2 + \rho_e^2 + 2\rho\rho_e \cos\varphi'} = \sqrt{z^2 + (\rho + \rho_e)^2 - 2\rho\rho_e \{1 - \cos\varphi'\}}$$

$$= \sqrt{z^2 + (\rho + \rho_e)^2 - 4\rho\rho_e \sin^2(\varphi'/2)}$$

gives

$$A_{e\varphi} = \frac{\varepsilon I_m}{2\pi\rho} \int_0^{\pi/2} \left[\frac{\left\{z^2 + (\rho + \rho_e)^2 - 2\rho\rho_e\right\}}{\sqrt{z^2 + (\rho + \rho_e)^2 - 4\rho\rho_e \sin^2\theta}} - \sqrt{z^2 + (\rho + \rho_e)^2 - 4\rho\rho_e \sin^2\theta} \right] d\theta$$

$$= \frac{\varepsilon I_m}{\pi} \sqrt{\frac{\rho_e}{\rho}} \frac{1}{k} \int_0^{\pi/2} \left[\frac{(1 - k^2/2)}{\sqrt{1 - k^2 \sin^2\theta}} - \sqrt{1 - k^2 \sin^2\theta} \right] d\theta$$

where

$$k = \frac{2\sqrt{\rho\rho_e}}{\sqrt{(\rho_e + \rho)^2 + z^2}}$$

Thus, we find

$$A_{e\varphi} = \frac{\varepsilon I_m}{\pi} \sqrt{\frac{\rho_e}{\rho}} \left[(1 - k^2/2)\, K(k) - E(k)\right]/k$$

where the complete elliptic integrals are defined by

$$K(k) = \int_0^{\pi/2} d\theta / \sqrt{1 - k^2 \sin^2\theta}$$

and

$$E(k) = \int_0^{\pi/2} d\theta \sqrt{1 - k^2 \sin^2\theta}$$

Note that these results can also be found from duality from the electric current loop [5].

4 CAPACITANCE

From the definition of the electric vector potential and Stoke's law, we can find the surface charge as

$$Q = \int_S \underline{n} \cdot \underline{D} \, dS = - \oint_C \underline{A}_e \cdot \underline{d\ell}$$

where the contour C encloses the surface S in a positive sense (counterclockwise) with respect to the normal $\underline{n}$. We want the charge (or electric flux) through the loop from the center out to radius $\rho_e - r_e$, where r_e will be found in the next section. (Note that in Figure 2, ρ_e is the average radius of the magnetic current loop with thickness $2r_e$.) In this axisymmetric case we have

$$Q = -2\pi \left(\rho_e - r_e\right) A_{e\varphi} \left(\rho_e - r_e, 0\right)$$

$$= -2\varepsilon I_m \sqrt{\rho_e \left(\rho_e - r_e\right)} \left[\left(1 - k_e^2/2\right) K\left(k_e\right) - E\left(k_e\right)\right] / k_e$$

where

$$k_e = \frac{\sqrt{\rho_e \left(\rho_e - r_e\right)}}{\left(\rho_e - r_e/2\right)}$$

The magnetic current (which includes an image in the ground plane of the actual gap problem) is related to the gap voltage V (positive on the center electrode) by means of

$$I_m = -2V$$

The capacitance of the antenna is thus taken as

$$C = Q/V = 4\varepsilon \sqrt{\rho_e \left(\rho_e - r_e\right)} \left[\left(1 - k_e^2/2\right) K\left(k_e\right) - E\left(k_e\right)\right] / k_e$$

4.1   Thin Gap

The case where the gap is thin $r_e/\left(2\rho_e\right) << 1$ allows us to expand the result by means of

$$k_e = 1 + O\left(k_e'^2\right) = 1 + O\left[r_e^2/\left(4\rho_e^2\right)\right]$$

$$k_e' = \sqrt{1 - k_e^2} = \frac{r_e}{2\rho_e - r_e} << 1$$

$$E\left(k_e\right) = 1 + O\left(k_e'^2\right) = 1 + O\left[r_e^2/\left(4\rho_e^2\right)\right]$$

$$K\left(k_e\right) = \ln\left(4/k_e'\right) + O\left(k_e'^2\right) = \ln\left\{4\left(2\rho_e/r_e - 1\right)\right\} + O\left[r_e^2/\left(4\rho_e^2\right)\right]$$

Then

$$C = 2\varepsilon \sqrt{\rho_e \left(\rho_e - r_e\right)} \left[\ln\left\{4\left(2\rho_e/r_e - 1\right)\right\} - 2\right] + O\left[r_e^2/\left(4\rho_e^2\right)\right]$$

$$\sim 2\varepsilon\rho_e \left[\ln\left(8\rho_e/r_e\right) - 2\right]$$

Again this expression can be obtained by duality from the inductance of an electric current loop [5].

φ = v/2

g/2

φ = 0
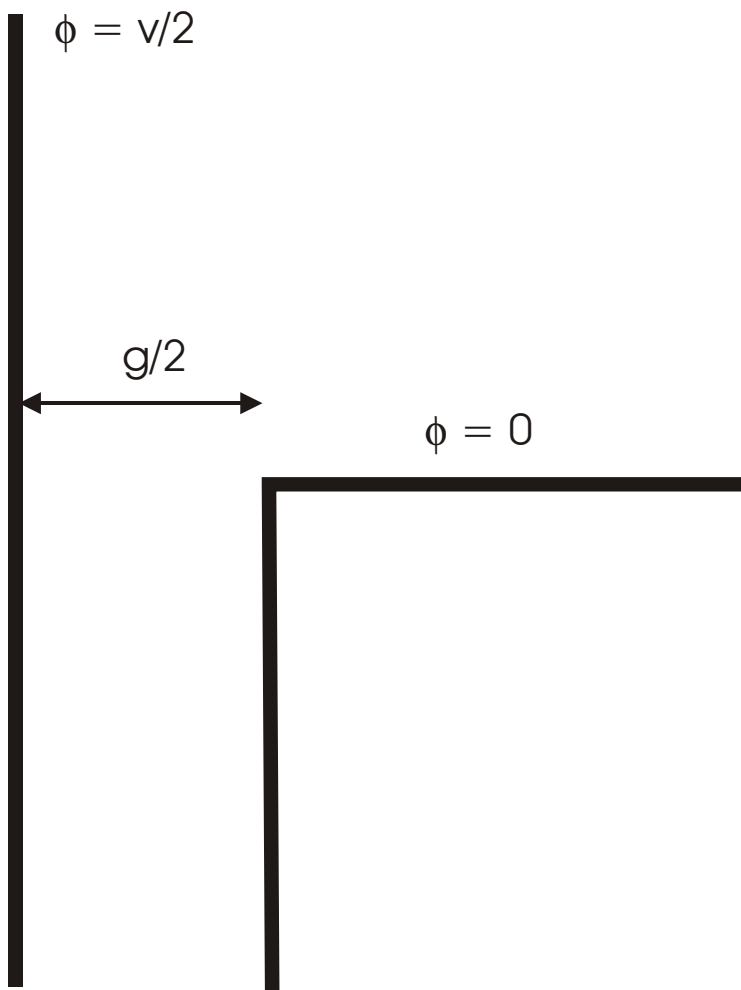
Figure 3. Narrow gap with symmetry plane (complex z-plane).

5 CONFORMAL MAPPING SOLUTION FOR A NARROW GAP

To choose the effective radius of the gap r_e we examine the conformal mapping solution of Figure 3 where the gap is

$$g = b - a$$

The Schwarz transformation which maps the upper half of a $z_1 = x_1 + iy_1$ plane into the region between the conductors with $z = x + iy$ (note when two-dimensional conformal mapping solutions are being considered, z will denote a complex variable rather than the axial coordinate) of Figure 2 is

$$\frac{dz}{dz_1} = C_1 z_1^{-1} (z_1 - 1)^{1/2}$$

The constant C_1 is evaluated by expanding near the singular point $z_1 = 0$

$$dz \sim iC_1 dz_1/z_1$$

and letting $z_1 = \delta e^{i\theta}$

$$dz \sim -C_1 d\theta$$

Thus when integrated near the singular point, we find

$$g/2 = C_1 \pi$$

Integration of the transformation then gives

$$z = \frac{g}{\pi} \left[\sqrt{z_1 - 1} - \arctan \sqrt{z_1 - 1} \right] + C_2$$

Let us choose $C_2 = g/2$ so that $z = g/2$ when $z_1 = 1$. Then the transformation becomes

$$z = g/2 + \frac{g}{\pi} \left[\sqrt{z_1 - 1} - \arctan \sqrt{z_1 - 1} \right]$$

The inverse tangent function is interpreted as

$$\arctan w = \frac{i}{2} \ln \left(\frac{i+w}{i-w} \right) = \frac{i}{2} \ln \left| \frac{i+w}{i-w} \right| + \frac{1}{2} (\theta_+ - \theta_-)$$

$$= \frac{i}{2} \ln \sqrt{\frac{u^2 + (v+1)^2}{u^2 + (v-1)^2}} + \frac{1}{2} \left[\pi - \text{Arctan} \left(\frac{1-v}{u} \right) \right] - \frac{1}{2} \text{Arctan} \left(\frac{v+1}{u} \right) , u > 0$$

where θ_+ is the angle made by the vector from the point w to the point i and θ_- is the angle made from the point $-i$ to the point w and

$$w = u + iv = \sqrt{z_1 - 1}$$

Note that the function Arctan is the principal branch [6] with $-\pi/2 < \text{Arctan}(x) < \pi/2$.

The electric field solution can be written in terms of the scalar potential ϕ

$$\underline{E} = -\nabla \phi$$

Gauss's law in regions free of electric charge ρ_v

$$\nabla \cdot \underline{D} = \rho_v = 0$$

gives Laplace's equation

$$\nabla^2 \phi = 0$$

The solution to Laplace's equation is taken as

$$\phi = \text{Im} (W)$$

where the complex potential is

12

$$W = \frac{V}{2\pi} \ln z_1$$

and the principal branch is used for the logarithm [6]. It is convenient now to return to the vector potential to obtain the charge on the conductors. The vector potential can be found as

$$A_{ez} = -\varepsilon \operatorname{Re}(W)$$

and the charge per unit length can be written as the unit length charge out to a radius R from the center and down to a distance R_0 from the center minus the charge per unit length at the right corner. Thus, in terms of the vector potentials,

$$q = A_{ez}(g/2, -R_0) - A_{ez}(R, 0)$$

$$= \varepsilon \operatorname{Re}\left[W(z = R) - W(z = g/2 - iR_0)\right]$$

$$= \frac{\varepsilon V}{2\pi} \ln \left| \frac{z_1(z = R)}{z_1(z = g/2 - iR_0)} \right|$$

Now let us expand the conformal transformation for large R ($z_1 = x_1 \to +\infty$) and R_0 ($z_1 = x_1 \to +0$)

$$z_1 = x_1 \sim (\pi R/g)^2$$

$$z_1 = x_1 \sim \exp\left[-2(1 + \pi R_0/g - \ln 2)\right]$$

Thus

$$q \sim \frac{\varepsilon V}{\pi}\left[\ln(\pi R/g) + 1 + \pi R_0/g - \ln 2\right]$$

The total charge from the conformal mapping solution is then

$$Q_{cm} = 2\pi \rho_e q \sim 2\varepsilon V \rho_e \left[\ln(\pi R/g) + 1 + \pi R_0/g - \ln 2\right]$$

The charge $\varepsilon V 2\pi \rho_e R_0/g$ results from the capacitance of the thin gap and is already accounted for by the coaxial capacitance of the transmission line. The charge $2\pi \rho_e \varepsilon (V/\pi) \ln R$, as R varies, is the charge accumulated from the field of a magnetic line current at the center of the gap $E \sim V/(\pi R)$. Taking $R = r_e$, and dividing by V we find the capacitive correction from the conformal mapping correction

$$\Delta C \sim 2\varepsilon \rho_e \left[\ln(\pi r_e/g) + 1 - \ln 2\right]$$

This solution tracks the field from its line current form down to the distance where the gap geometry influences the field and the total charge. Adding this to the previous expression for the loop capacitance gives

$$C \sim 2\varepsilon \rho_e \left[\ln(4\pi \rho_e/g) - 1\right]$$

Note that this result can also be viewed as taking

$$r_e = \frac{2g}{\pi e} \approx \frac{g}{4.27}$$

This value is not far from the well known result $g/4$ for the equivalent radius of a narrow planar slot of width g in a thin plane [7].

6 AVERAGING APPROXIMATION FOR AXISYMMETRIC PROBLEM

The effective radius of the loop can be approximated for small gaps by

$$\rho_e \approx (b + a)/2$$

An improvement can be made in the preceding capacitance result by noting that for small a/b we would expect the field to have an overall (aside from the local edge singularities) behavior given by

$$E_\rho \approx \frac{V}{\rho \ln (b/a)} = -K_{m\varphi}/2 \,, \quad a < \rho < b$$

where the magnetic surface current is $K_{m\varphi}$. This motivates setting the radius of the magnetic current filament to the average radius of the magnetic surface current

$$\rho_e = \frac{1}{I_m} \int_a^b K_{m\varphi} \rho d\rho = \frac{b - a}{\ln (b/a)}$$

Note that this result approaches $(b + a)/2$ as $b \to a$. It is less than this value otherwise, shrinking to small values as $a \to 0$ (which is expected, since the magnetic current is concentrated about the inner electrode for this limit). Inserting this value into the preceding capacitance formula gives

$$C \approx 2\varepsilon \frac{b - a}{\ln (b/a)} \left[\ln \left\{ 4\pi / \ln (b/a) \right\} - 1 \right] \approx (0.1604 \text{ pF}) \, \varepsilon / \varepsilon_0$$

where the final numerical value is for the dimensions given previously.

This formula turns out to be remarkably accurate for a wide range of a/b ratios, as will be illustrated below (it eventually fails for $a/b \to 0$ and, in fact, becomes negative). A result from [8]

$$C_{lp} \approx 8\varepsilon \frac{b + a}{\ln^2 (b/a)} \left[E \left(\frac{2\sqrt{ab}}{b + a} \right) - 1 \right]$$

will also be used for comparison purposes. This result is from a variational expression for the admittance and a $E_\rho \approx V/\left\{ \rho \ln (b/a) \right\}$ trial function. This result becomes $C \sim 4\varepsilon b \left(\pi - 2 \right) / \ln^2 (b/a)$ as $a/b \to 0$ and thus may be more accurate for small values of a.

6.1 Numerical Comparisons

Based on an analysis presented in [9], very accurate numerical computations were performed on the probe. With an inner and outer radii given by

$$a \approx 0.121 \text{ in}$$

and

$$b \approx 0.189 \text{ in},$$

the result for the admittance at 1 GHz was

$$Y_a \approx -i1.005 \left(\varepsilon / \varepsilon_0 \right) \text{ mS at 1 GHz}$$

The capacitance was thus

$$C_a \approx Y_a / \left(-i\omega \right) \approx 0.1600 \left(\varepsilon / \varepsilon_0 \right) \text{ pF}$$

This result is quite close to the value in the preceding formula from the averaging approximation

$$C \approx 0.1604 \left(\varepsilon / \varepsilon_0 \right) \text{ pF}$$

Another axisymmetric code, based on a boundary value formulation for the magnetic fields at the antenna surface (or, equivalently, the transmission line termination)[10], was also run as a check. The value obtained by this computation was

$$C_n \approx 0.1601 \left(\varepsilon / \varepsilon_0 \right) \text{ pF}$$

This code was run at several values of a/b and a comparison between the values obtained versus the averaging approximations above is shown in Figure 4. Here it is evident that above about $a/b > 0.1$, the formula yields quite accurate results. Also shown is the result from the variational expression given in [8].

As an additional check on the analytic result for the capacitance, the computation based on [9] was also performed for a fifty ohm coaxial antenna with dimensions

$$a = 0.635 \text{ mm}$$

$$b = 1.462 \text{ mm}$$

The accurate computation at 1 GHz [9] gave

$$Y_a \approx -i0.1878 \left(\varepsilon / \varepsilon_0 \right) \text{ mS at 1 GHz}$$

or

$$C_a \approx Y_a / \left(-i\omega \right) \approx 0.0299 \left(\varepsilon / \varepsilon_0 \right) \text{ pF}$$

The above averaging formula gives

$$C \approx 0.0308 \left(\varepsilon / \varepsilon_0 \right) \text{ pF}$$

which is again quite an accurate estimate. The axisymmetric code based on the boundary integral equation method [10] gave
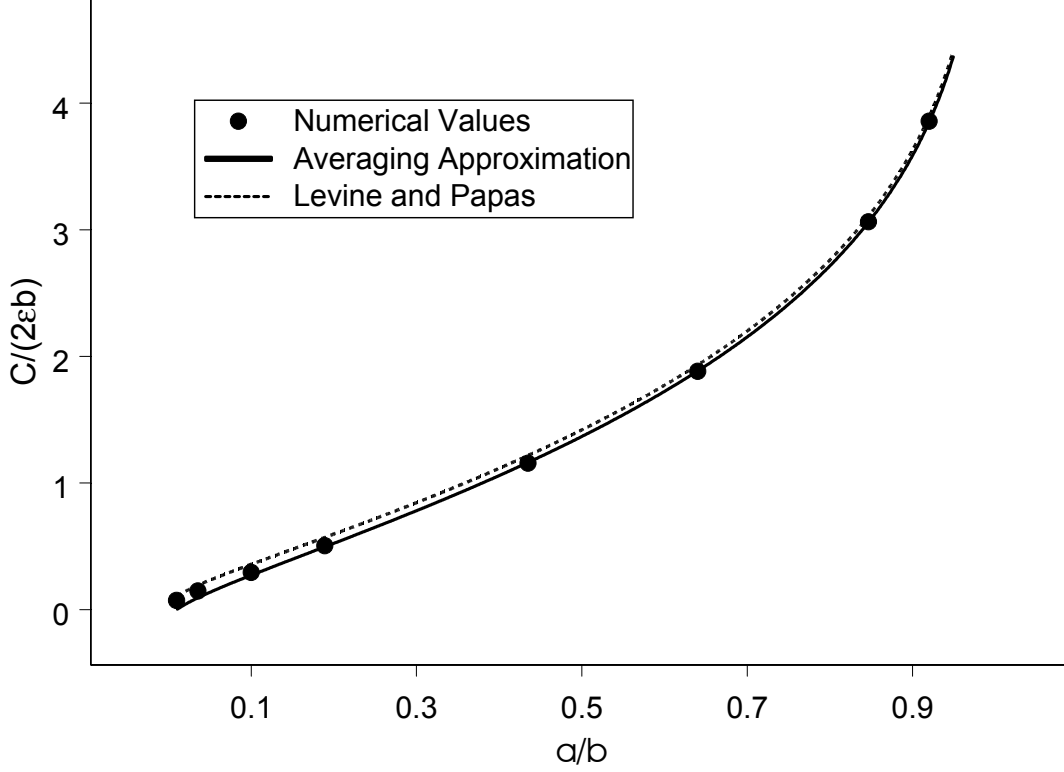
Figure 4. Comparison of simple logarithmic capacitance formula with "averaged" gap radius and numerical simulations. The variational expression is also shown.

$$C_n \approx 0.0299 \left(\varepsilon / \varepsilon_0 \right) \text{ pF}$$

7 ROUNDED CORNERS

Because of the effectiveness of using the average circumference to normalize two-dimensional quantities from conformal mapping, we can also treat more detailed features associated with the probe construction by means of conformal mapping. The actual probe has rounded corners with radius of curvature

$$\rho_0 = 0.031 \text{ in}$$

as shown in Figure 5. The method in Smythe [11] or Carrier [12] is used to round the corner. This method is simply to replace the factor $(z_1 - 1)^{\alpha/\pi - 1}$ in the Schwarz transformation by the sum of two singular point factors $(z_1 - \lambda)^{\alpha/\pi - 1} + \kappa (z_1 - 1)^{\alpha/\pi - 1}$ where κ can be used to adjust the shape of the curve between the points and $0 < \lambda < z_1 = x_1 < 1$. Thus, in this case the Schwarz transformation becomes
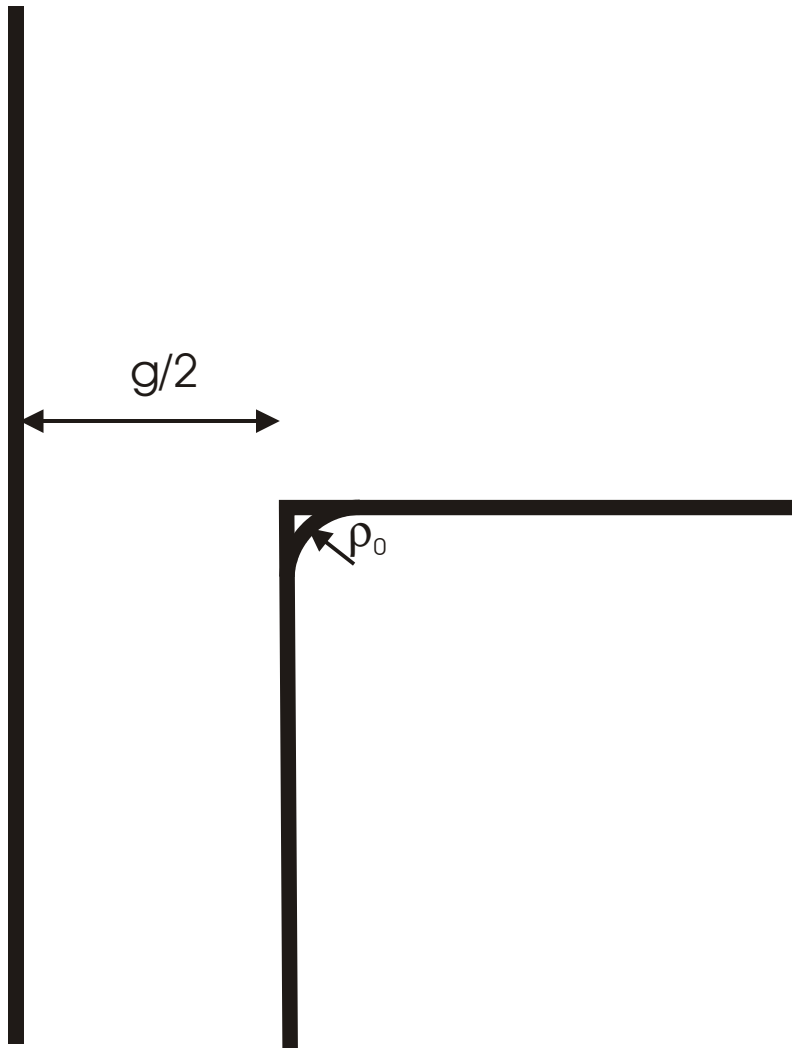
Figure 5. Rounded corner two-dimensional complex z-plane geometry with symmetry plane in middle of gap.

$$\frac{dz}{dz_1} = C_1 z_1^{-1} \left[\sqrt{z_1 - \lambda} + \kappa \sqrt{z_1 - 1} \right]$$

The evaluation of the constant C_1 proceeds as before with the expansion near the $z_1 = 0$ singular point

$$dz \sim iC_1 \left(\lambda^{1/2} + \kappa \right) \frac{dz_1}{z_1} , \; z_1 \to 0$$

Letting $z_1 = \delta e^{i\theta}$ and $dz_1/z_1 = id\theta$ gives

$$dz \sim -C_1 \left(\lambda^{1/2} + \kappa \right) d\theta$$

Integration from $\theta = 0$ to $\theta = \pi$ gives

$$-g/2 = -C_1 \left(\lambda^{1/2} + \kappa \right) \pi$$

or

$$C_1 = \frac{g}{2\pi \left(\lambda^{1/2} + \kappa \right)}$$

Integration of the transformation yields

$$z = C_2 + \frac{g}{\pi \left(\lambda^{1/2} + \kappa \right)} \left[\sqrt{z_1 - \lambda} - \lambda^{1/2} \arctan \sqrt{z_1/\lambda - 1} \right]$$

$$+ \frac{g\kappa}{\pi \left(\lambda^{1/2} + \kappa \right)} \left[\sqrt{z_1 - 1} - \arctan \sqrt{z_1 - 1} \right]$$

Assuming all parameters are real we see that $\text{Im}(z) = 0$ when $z_1 = x_1 > 1$.

Now we want to enforce the two equations (so that we return to the original boundary contour outside of the smoothed region)

$$g/2 + \rho_0 = C_2 + \frac{g}{\pi \left(\lambda^{1/2} + \kappa \right)} \left[\sqrt{1 - \lambda} - \lambda^{1/2} \text{Arctan} \sqrt{1/\lambda - 1} \right]$$

$$g/2 - i\rho_0 = C_2 + \frac{g\kappa}{\pi \left(\lambda^{1/2} + \kappa \right)} \left[i\sqrt{1 - \lambda} - i\text{Arctanh} \sqrt{1 - \lambda} \right]$$

where $\text{Arctanh}(x) = \frac{1}{2} \ln \left(\frac{1+x}{1-x} \right)$ denotes the principal value [6]. Now choosing

$$C_2 = g/2$$

gives

$$\rho_0 = \frac{g}{\pi \left(\lambda^{1/2} + \kappa \right)} \left[\sqrt{1 - \lambda} - \lambda^{1/2} \text{Arctan} \sqrt{1/\lambda - 1} \right]$$

$$-\rho_0 = \frac{g\kappa}{\pi\left(\lambda^{1/2} + \kappa\right)}\left[\sqrt{1-\lambda} - \operatorname{Arctanh}\sqrt{1-\lambda}\right]$$

or

$$\sqrt{1-\lambda} - \lambda^{1/2}\operatorname{Arctan}\sqrt{1/\lambda - 1} = -\kappa\left[\sqrt{1-\lambda} - \operatorname{Arctanh}\sqrt{1-\lambda}\right]$$

$$\pi\left(\lambda^{1/2} + \kappa\right)\frac{\rho_0}{g}(1 + 1/\kappa) = \operatorname{Arctanh}\sqrt{1-\lambda} - \lambda^{1/2}\operatorname{Arctan}\sqrt{1/\lambda - 1}$$

Also, for $0 < z_1 = x_1 < \lambda$, we see that $x = g/2$ and $y < 0$. In addition, for $z_1 = x_1 < 0$, we see that $x = 0$.

Thus the transformation is

$$z = g/2 + \frac{g}{\pi\left(\lambda^{1/2} + \kappa\right)}\left[\sqrt{z_1 - \lambda} - \lambda^{1/2}\arctan\sqrt{z_1/\lambda - 1}\right]$$

$$+\frac{g\kappa}{\pi\left(\lambda^{1/2} + \kappa\right)}\left[\sqrt{z_1 - 1} - \arctan\sqrt{z_1 - 1}\right]$$

with equations

$$\kappa = -\frac{\sqrt{1-\lambda} - \lambda^{1/2}\operatorname{Arctan}\sqrt{1/\lambda - 1}}{\sqrt{1-\lambda} - \operatorname{Arctanh}\sqrt{1-\lambda}}$$

and

$$\pi\left(\lambda^{1/2} + \kappa\right)\frac{\rho_0}{g}(1 + 1/\kappa) = \operatorname{Arctanh}\sqrt{1-\lambda} - \lambda^{1/2}\operatorname{Arctan}\sqrt{1/\lambda - 1}$$

Eliminating κ gives the equation

$$F(\lambda) = \frac{1}{\sqrt{1/\lambda - 1} - \operatorname{Arctan}\sqrt{1/\lambda - 1}} - \frac{1}{\sqrt{1-\lambda} - \operatorname{Arctanh}\sqrt{1-\lambda}} = \frac{g}{\pi\rho_0} \approx 0.6982$$

where the final numerical value uses the above parameter values. Some values of $F(\lambda)$ are

$$F(0.5) = 10.4$$

$$F(0.25) = 3.678$$

$$F(0.1) = 1.721$$

$$F(0.015) = 0.7068$$

$$F(0.01) = 0.6184$$

The proper value is near
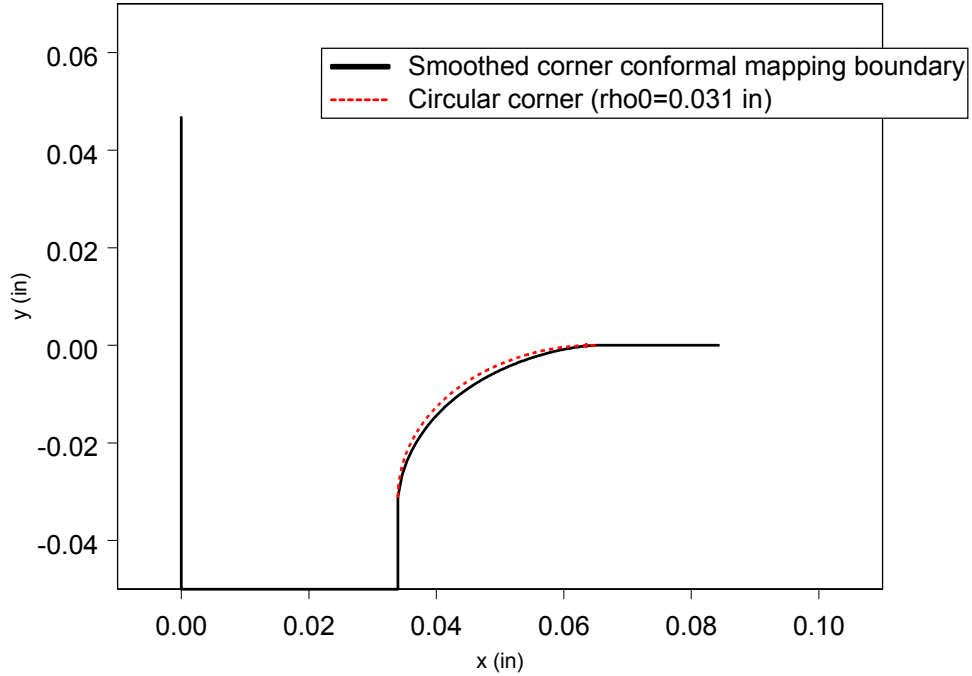
Figure 6. Two-dimensional boundary with "smoothed" conformal transformation corner versus a circular corner.

$$F\left(\lambda \approx 0.01448\right) = 0.6983$$

which gives

$$\kappa \approx 0.4510$$

The solution for the probe dimensions to many digits is

$$\lambda = 0.0144785898607$$

$$\kappa = 0.450990368302$$

The boundary of the two-dimensional "smoothed" corner is compared against a circular corner in Figure 6. The agreement is reasonable.

The potential solution is found as in preceding section

$$\phi = \text{Im}\left(W\right)$$

where

$$W = \frac{V}{2\pi} \ln z_1$$

and

$$A_{ez} = -\varepsilon \, \text{Re}\,(W)$$

We need the expansion of the conformal transformation for $z_1 = x_1$ near the origin and near infinity. Near infinity we let $x = R$

$$\sqrt{x_1} \sim \frac{\lambda^{1/2} + \kappa}{1 + \kappa} \pi R/g$$

Near the origin we let $x = g/2$ and $y = -R_0$ to obtain

$$-R_0 = \frac{g}{\pi \left(\lambda^{1/2} + \kappa \right)} \left[\sqrt{\lambda - x_1} - \lambda^{1/2} \frac{1}{2} \ln \left(\frac{1 + \sqrt{1 - x_1/\lambda}}{1 - \sqrt{1 - x_1/\lambda}} \right) \right]$$

$$+ \frac{g\kappa}{\pi \left(\lambda^{1/2} + \kappa \right)} \left[\sqrt{1 - x_1} - \frac{1}{2} \ln \left(\frac{1 + \sqrt{1 - x_1}}{1 - \sqrt{1 - x_1}} \right) \right]$$

$$\sim \frac{g}{\pi} \left[1 + \frac{1}{2} \ln (x_1/4) \right] - \frac{g\lambda^{1/2} \ln \lambda}{2\pi \left(\lambda^{1/2} + \kappa \right)}$$

or

$$-\frac{1}{2} \ln (x_1) \sim 1 - \ln 2 + \pi R_0/g - \frac{\lambda^{1/2} \ln \lambda}{2 \left(\lambda^{1/2} + \kappa \right)}$$

where this minus the charge per unit length on the wall is then

$$q = \frac{\varepsilon V}{2\pi} \ln \left| \frac{z_1 \, (z = R)}{z_1 \, (z = g/2 - iR_0)} \right|$$

$$\sim \varepsilon \frac{V}{\pi} \left[\ln \left(\frac{\lambda^{1/2} + \kappa}{1 + \kappa} \pi R/g \right) + 1 - \ln 2 + \pi R_0/g - \frac{\lambda^{1/2} \ln \lambda}{2 \left(\lambda^{1/2} + \kappa \right)} \right]$$

The total charge from the rounded corner solution is

$$Q_{rc} = 2\pi \rho_e q \sim 2\varepsilon V \rho_e \left[\ln \left(\frac{\lambda^{1/2} + \kappa}{1 + \kappa} \pi R/g \right) + 1 - \ln 2 + \pi R_0/g - \frac{\lambda^{1/2} \ln \lambda}{2 \left(\lambda^{1/2} + \kappa \right)} \right]$$

Again we drop the $2\pi \rho_e V R_0/g$ contribution since this is already included in the coaxial capacitance. Dividing by V and letting $R = r_e$, we obtain

$$\Delta C_{rc} \sim 2\varepsilon \rho_e \left[\ln \left(\frac{\lambda^{1/2} + \kappa}{1 + \kappa} \pi r_e/g \right) + 1 - \ln 2 - \frac{\lambda^{1/2} \ln \lambda}{2 \left(\lambda^{1/2} + \kappa \right)} \right]$$

where adding this to the capacitance of the loop gives the capacitance with the rounded corner

$$C_{rc} \sim 2\varepsilon\rho_e \left[\ln\left(4\pi\rho_e/g\right) - 1 + \ln\left(\frac{\lambda^{1/2} + \kappa}{1 + \kappa}\right) - \frac{\lambda^{1/2}\ln\lambda}{2\left(\lambda^{1/2} + \kappa\right)} \right]$$

Thus, the correction capacitance for the rounded corner is

$$C_{rc} - C = 2\varepsilon\rho_e \left[\ln\left\{ \frac{\left(\lambda^{1/2} + \kappa\right)}{(1 + \kappa)} \right\} - \frac{\lambda^{1/2}\ln\lambda}{2\left(\lambda^{1/2} + \kappa\right)} \right] \approx 2\varepsilon\rho_e\left(-0.486055\right)$$

The value to many digits is

$$C_{rc} - C = 2\varepsilon\rho_e\left(-0.48607428756\right)$$

Using the averaged circumference, we have

$$C_{rc} - C = 2\varepsilon\frac{b-a}{\ln\left(b/a\right)} \left[\ln\left(\frac{\lambda^{1/2} + \kappa}{1 + \kappa}\right) - \frac{\lambda^{1/2}\ln\lambda}{2\left(\lambda^{1/2} + \kappa\right)} \right] \approx -0.0333\left(\varepsilon/\varepsilon_0\right) \text{ pF}$$

and adding this to the previous value of the capacitance with sharp corners, we obtain

$$C_{rc} \approx 0.1271\left(\varepsilon/\varepsilon_0\right) \text{ pF}$$

7.1   Approximate Solution of Mapping Parameters

It is easy to approximate the transcendental equation in this case. Suppose we approximate $F\left(\lambda\right)$ for small λ as

$$F\left(\lambda\right) \sim \sqrt{\lambda} - \frac{1}{1 + \frac{1}{2}\ln\left(\lambda/4\right)} \approx \frac{g}{\pi\rho_0}$$

Solving iteratively, we find

$$\ln\left(\lambda/4\right) \approx -2\frac{\pi\rho_0}{g}\left[1 + \sqrt{\lambda}\frac{\pi\rho_0}{g}\right] - 2$$

$$\approx -2\frac{\pi\rho_0}{g}\left(1 + \frac{2\pi\rho_0}{ge^{1+\pi\rho_0/g}}\right) - 2$$

or

$$\lambda \approx 4/\exp\left[\left(1 + e^{-1-\pi\rho_0/g}2\pi\rho_0/g\right)2\pi\rho_0/g + 2\right] \approx 0.0150$$

where the final numerical value is for the above probe parameters. The value of κ is then given by

$$\kappa \sim -\frac{1 - \sqrt{\lambda}\pi/2}{1 + \frac{1}{2}\ln(\lambda/4)} \approx 0.4505$$

These results are quite close to the above accurate numerical values. The correction capacitance is then

$$C_{rc} - C = 2\varepsilon\rho_e \left[\ln\left\{ \frac{\left(\lambda^{1/2} + \kappa\right)}{(1 + \kappa)} \right\} - \frac{\lambda^{1/2}\ln\lambda}{2\left(\lambda^{1/2} + \kappa\right)} \right] \approx 2\varepsilon\rho_e\left(-0.4798\right)$$

again quite close to the preceding exact values.

7.2 Numerical Comparisons with Rounded Corners

The axisymmetric code mentioned in the preceding section [10] was also run on the circular corner geometry. This code used a stairstep approximation for the corner profile. Several cases were run and extrapolation to the limit was used to obtain

$$C \approx (0.1271)\left(\varepsilon/\varepsilon_0\right) \text{ pF}$$

which is very close to the preceding conformal mapping result. In fact this may be *too close* given the approximation to the circular corner afforded by the smoothing transformation in the conformal mapping (more will be said about this in the effective area comparison section presented below).

8 EFFECTIVE AREA

A uniform z - directed field E_0 is taken above the ground plane. The received charge, when the transmission line is short circuited, is written in terms of the effective area A_e by means of

$$Q_r = A_e\epsilon E_0$$

where the effective area is written in terms of the effective radius by means of

$$A_e = \pi\rho_e^2$$

(Note that this definition is different than the commonly-used effective area definition of an antenna, which is related to the antenna directivity). The value of the effective radius is taken to be the same as the average above

$$A_e \approx \pi\frac{(b - a)^2}{\ln^2(b/a)} \approx 0.6509\,\pi b^2$$

The short circuit current is thus given by

$$I_{sc} = \frac{\partial Q_r}{\partial t}$$

Note that reciprocity can also be used to derive a result from the $E_\rho = A/\left\{\rho\ln(b/a)\right\}$ assumption [13],

[14]. This gives

$$A_e^r \approx \pi \frac{(b^2 - a^2)}{2 \ln (b/a)}$$

This formula turns out to not be as accurate as the preceding results.

8.1   Numerical Comparisons

From [9], very accurate numerical values were computed for the effective height of the straight-edge corner antenna (without rounded edges) of dimensions

$$a \approx 0.121 \text{ in}$$

$$b \approx 0.189 \text{ in}$$

The result at 1 GHz for the probe geometry was

$$h_e^a/a \approx 0.8393$$

where the effective area is related by

$$A_e^a = h_e^a \left(C_a/\varepsilon\right) \approx 0.6439 \pi b^2$$

Using the average ρ_e formula, the effective area becomes

$$A_e \approx 0.6509 \, \pi b^2$$

and is quite an accurate estimate. As a check, the boundary-value axisymmetric code [10] was also run for the effective height of the straight-edge corner antenna. The value obtained by this computation was

$$A_e^n \approx 0.6445 \pi b^2$$

This code was also run for several values of a/b and compared with the above formula as shown in Figure 8. The above formula is an accurate approximation above about $a/b > 0.1$. The dashed curve is the result from reciprocity and the $E_\rho = V / \{\rho \ln (b/a)\}$ assumption.

As done with the capacitance results, another check of the effective height was also performed for a fifty ohm coaxial antenna with dimensions

$$a = 0.635 \text{ mm}$$

$$b = 1.462 \text{ mm}$$

The accurate computation at 1 GHz gave [9]
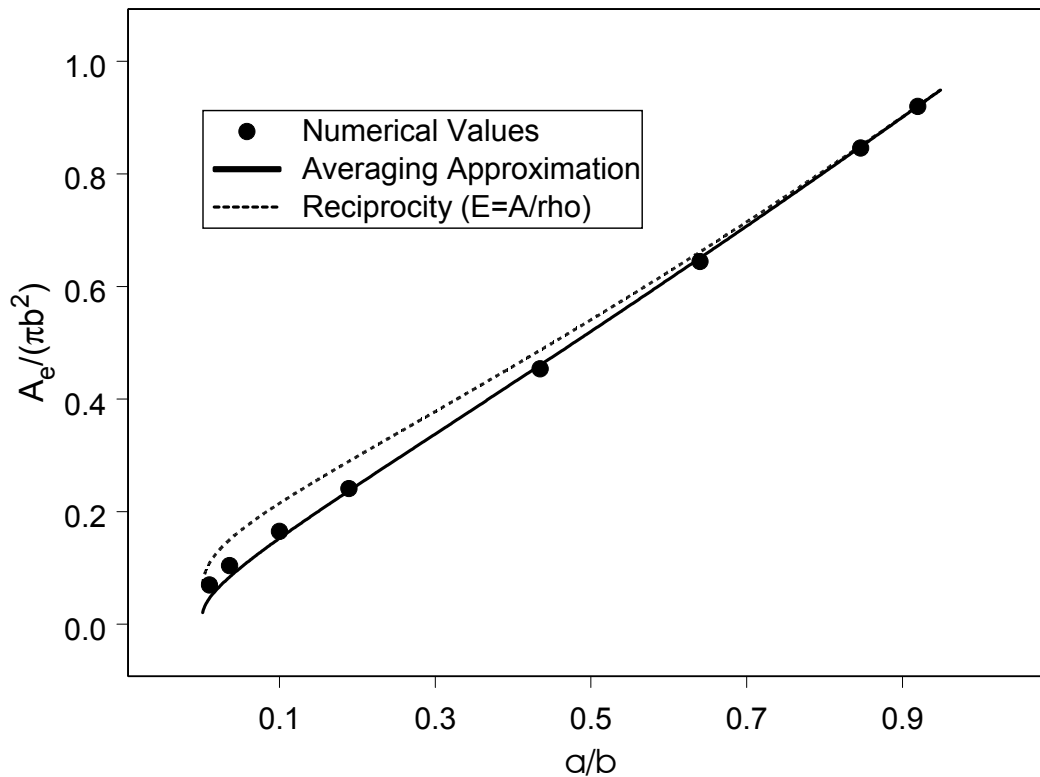
$$h_e^a/a = 1.419$$

or

Figure 7. Comparison of numerical and averaged formula for effective area. Also shown as the dashed curve is the reciprocity result using the $E_\rho = V/\{\rho \ln(b/a)\}$ assumption.

$$A_e^a = h_e^a \left(C_a/\varepsilon\right) \approx 0.4530\pi b^2$$

The above approximate formula gives

$$A_e \approx 0.4601\pi b^2$$

which is again an accurate estimate. The axisymmetric code based on [10] gave

$$A_e^n \approx 0.4536\pi b^2$$

8.2 Rounded Corner Effective Area

The preceding axisymmetric code [10] was also used to estimate the effective area of the probe with circular corners. The result was

$$A_e \approx (0.6281)\,\pi b^2$$

This result is slightly less (2.5 %) than the numerical result for the flush probe and is also slightly less (3.5 %) than the averaging approximation. Nevertheless the argument (valid in the two-dimensional Cartesian problem) for retaining approximately the same value of the effective area when the corners are rounded does seem justified (note in contrast that the capacitance reduction from the rounding is 20.6 %) and the averaging result is reasonably accurate.

An improvement can be otained by using a modified average radius. Because of the rounding we would expect the effective radius to be reduced because of charge rearrangement from the inner to outer conductors. The gap at the $z = 0$ plane is actually changed from the parameters (a, b) to a larger interval. Suppose we take this gap to be increased in each direction by half the corner radius to $(a - \rho_0/2,\, b + \rho_0/2)$. Then

$$\rho'_e = \frac{(b + \rho_0/2) - (a - \rho_0/2)}{\ln\left[(b + \rho_0/2)/(a - \rho_0/2)\right]}$$

This modification gives

$$A'_e = \pi \rho'_e \approx (0.6264)\,\pi b^2$$

which is quite an accurate result.

Note that if we had used this effective radius in the capacitance formulas we would obtain

$$C'_{rc} \approx 2\varepsilon \rho'_e \left[\ln\left(4\pi\rho'_e/g\right) - 1 + \ln\left(\frac{\lambda^{1/2} + \kappa}{1 + \kappa}\right) - \frac{\lambda^{1/2}\ln\lambda}{2\left(\lambda^{1/2} + \kappa\right)}\right] \approx 0.1233 \text{ pF}$$

This is about 3% below the numerical value, however it may be more representative of the value associated with the profile afforded by the conformal smoothing transformation. If we recalculate the conformal mapping parameters with a slightly smaller value of $\rho_0 \to \rho_1 = 0.028$ in, the corner geometry comes closer to the desired circular geometry as shown in Figure 7. The corresponding conformal mapping parameters are

$$\lambda \approx 0.0193$$

$$\kappa = 0.4732$$

and capacitance change

$$C_{rc} - C \approx 2\varepsilon \rho_e\,(-0.4307)$$

The above formula with the new average radius gives

$$C_{rc} \approx 0.1271 \text{ pF}$$

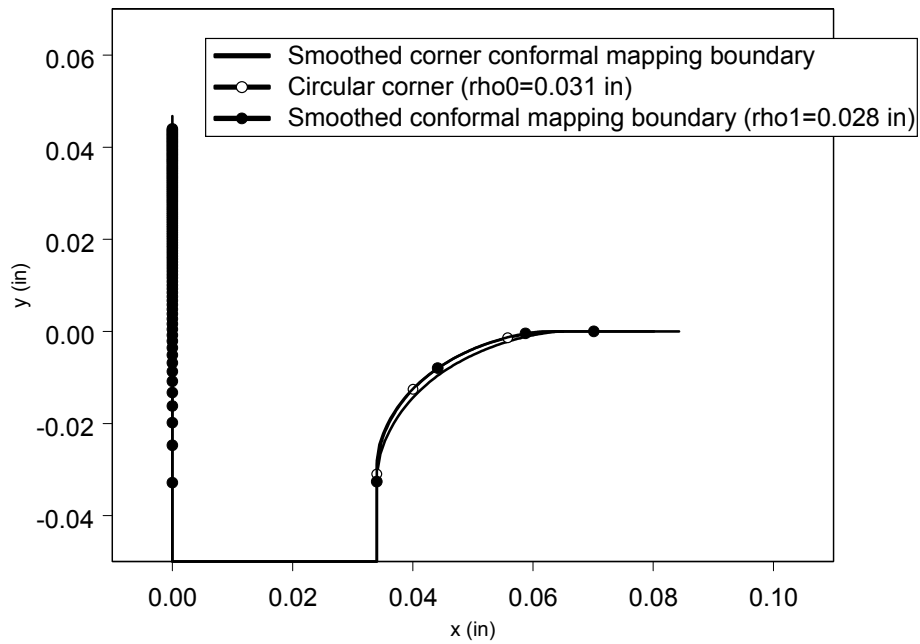This result is virtually identical to the numerical result.

26

Figure 8. Two-dimensional boundary with "smoothed" conformal transformation corner versus a circular corner. Here the conformal mapping results correspond to two different radii of curvature, with 0.028 in. representing a 'modified average' radius between the inner and outer conductors..

9 PROBE INTERIOR

The interior of the probe is shown in Figure 9. The medium of the half space extends down to height

$$h \approx 0.123 \text{ in}$$

below the ground plane. Assuming the following parameters for the terminating transmission line (RG214)

$$C_0 = 1/\left(vZ_0\right) \approx 101.08 \text{ pF/m}$$

$$Z_0 = 50 \text{ ohms}$$

$$v = 0.66c$$

we have a lumped capacitance correction for this region of

$$\Delta C_{coax} = \left\{ \frac{2\pi\varepsilon}{\ln\left(b/a\right)} - C_0 \right\} h \approx 31.02 \text{ pF}$$

Here the capacitance correction accounts for the difference between the capacitance in the water section of the D-dot probe and the transmission line capacitance. Similarly, the capacitance correction in the plastic region is estimated to be

$$\Delta C_{plastic} \approx \left(4.819 - C_0 \left(0.150 + 0.7 + 0.406 + 0.298\right) \ 0.0254\right) \approx 0.83 \text{ pF}$$

Here the value of 4.819 pF for the capacitance in the plastic regions is obtained as the parallel combinations of the coaxial capacitances from the water/dielectric interface down through the reference plane on the HN connector (shown in Figure 9). More specifically, the capacitance of the plastic section can be written in terms of the coaxial capacitances associated with the sylgard narrow and wide sections, the series combination of sylgard and silicone capacitances, and the silicone end section capacitance:

$$C_{plastic} = C_{sy \, \lg ard, Nar \, row} + C_{sy \, \lg ard, Wide} + C_{\text{series} \, Cap} + C_{endSection}$$

Note that corrections resulting from the right angle bends [15] can also be added here but was not done so since the contribution from the plastic region to the total capacitance was found to be relatively small in this case. In the case that the upper half space was air filled (instead of water filled), the contributions from the plastic region and consequently, the right angle bend corrections would be much more significant (to the extent where a redesign of the D-dot probe would probably be desired).

10 EXPERIMENT

In addition to the analytic and numerical simulations performed for the D-dot capacitance, the capacitance of the D-dot probe was also measured in a time harmonic experiment at $f = 1$ MHz . The total measured capacitance C_{tot} in these measurements included the C_0 of the coax from the connector reference plane to the ground plane. Mounting the D-dot probe flush into a 2.75 in diameter ground plane and using distilled water as the half-space medium, the measured total capacitance was recorded as
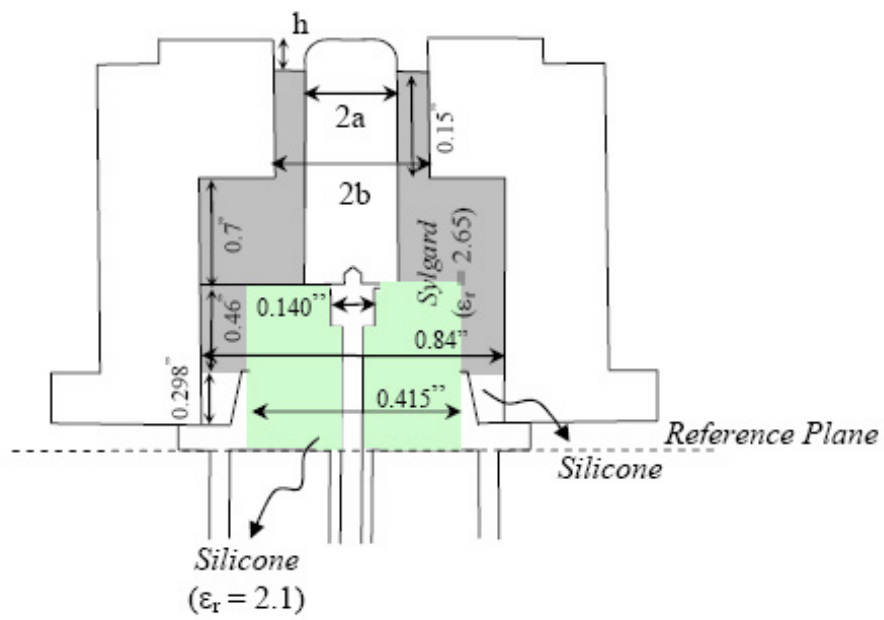
28

Figure 9. A cross-sectional view of the D-dot probe.

$$C_{tot,Measured} = 48.1 \text{ pF}$$

The total capacitance is related to the capacitance contributions discussed above as

$$C_{tot} = C + \Delta C_{corn} + \Delta C_{coax} + \Delta C_{plastic}$$

where, as given previously,

$$C = 2\varepsilon\rho_e \left[\ln\left(4\pi\rho_e/g\right) - 1\right] \approx (0.1604 \text{ pF}) \, \varepsilon/\varepsilon_0$$

and

$$\Delta C_{corn} = C_{rc} - C = 2\varepsilon \frac{b-a}{\ln(b/a)} \left[\ln\left(\frac{\lambda^{1/2}+\kappa}{1+\kappa}\right) - \frac{\lambda^{1/2}\ln\lambda}{2\left(\lambda^{1/2}+\kappa\right)}\right] \approx -0.0333 \left(\varepsilon/\varepsilon_0\right) \text{ pF}$$

Thus, using a value of

$$\varepsilon/\varepsilon_0 \approx 80.4 \text{ at } 20^o\text{C}$$

for distilled water and

$$h \approx 0.123 \text{ in}$$

the total calculated capacitance becomes

$$C_{tot} = 42.1 \text{ pF}$$

Thus, there is approximately a 12% difference between the measured and calculated capacitances. Here it is important to note that since the capacitance is extremely sensitive to the value of h (recall that for a water-filled upper half space, the coaxial capacitance correction is the dominant contribution to the overall capacitance), the height of the probe in the water region must be known to high precision. In this particular measurement, the distance from the ground plane to the plastic interface (h) was taken as the average distance measured circumferentially around the inner conductor since for the probe used in this measurement, the plastic interface was found to be slightly uneven around the circumference.

11 CONCLUSION AND SUMMARY

This report constructs simple models for capacitance and effective area (proportional to charge and short circuit current) of flush-mounted, monopole-type, low-frequency electric field probes. Conformal mapping has been used along with the introduction of a technique for choosing an average circumference, which allows the two-dimensional cross section results to be applied to the axisymmetric three-dimensional probes. Issues associated with rounded edges have also been addressed. Numerical axisymmetric calculations have been performed, confirming the accuracy and utility of the models. An experiment to determine the probe capacitance has also been carried out. The remainder of this section is a summary of the formulas and a discussion of how the results enter the circuit model for the probes. It is to be noted that for slowly-varying signals (low frequencies) and resistive loads (such as a fifty-ohm measurement system), the short- circuit current (which is determined by the effective area alone) dominates the response. The capacitance then determines the probe time constant and can be used in the circuit model to correct for rise time distortion.

Listed below are the steps necessary to compute the circuit-model parameters used to represent the D-dot probe. Also summarized are the calculations pertaining to the D-dot probe analyzed in this paper.

From the geometry of the antenna, set the effective radius and gap geometry parameters

$$a \approx 0.121 \text{ in}$$

$$b \approx 0.189 \text{ in}$$

$$\rho_e = \frac{b - a}{\ln(b/a)} \approx 0.1525 \text{ in}$$

$$g = b - a \approx 0.068 \text{ in}$$

The capacitance is

$$\varepsilon/\varepsilon_0 \approx 80.4 \text{ at } 20^o\text{C}$$

$$C \approx 2\varepsilon\rho_e \left[\ln(4\pi\rho_e/g) - 1\right] \approx 12.9 \text{ pF}$$

The effective area is

$$A_e \approx \pi\rho_e^2 \approx 4.71 \times 10^{-5} \text{ m}^2$$

The short circuit charge and current are then

$$Q = A_e\varepsilon E_0$$

$$I_{sc} = \frac{\partial}{\partial t}Q$$

The effective height is then

$$h_e = A_e/(C/\varepsilon) \approx 2.60 \times 10^{-3} \text{ m}$$

where the open circuit voltage V_{oc} is

$$V_{oc} = h_e E_0$$

For rounded corners of radius

$$\rho_0 \approx 0.031 \text{ in}$$

add the capacitance

$$\Delta C_{corn} = 2\varepsilon\rho_e \left[\ln\left(\frac{\sqrt{\lambda} + \kappa}{1 + \kappa}\right) - \frac{\sqrt{\lambda}\ln\lambda}{2\left(\sqrt{\lambda} + \kappa\right)}\right] \approx -2.68 \text{ pF}$$

where

$$\kappa = -\frac{\sqrt{1-\lambda} - \sqrt{\lambda}\operatorname{Arctan}\sqrt{1/\lambda - 1}}{\sqrt{1-\lambda} - \operatorname{Arctanh}\sqrt{1-\lambda}} \approx 0.451$$

and

$$F(\lambda) = \frac{1}{\sqrt{1/\lambda - 1} - \operatorname{Arctan}\sqrt{1/\lambda - 1}} - \frac{1}{\sqrt{1-\lambda} - \operatorname{Arctanh}\sqrt{1-\lambda}} = \frac{g}{\pi\rho_0} \approx 0.698$$

so that

$$\lambda \approx 0.0145$$

Or as approximation for $\lambda << 1$

$$\lambda \approx 4/\exp\left[\left(1 + e^{-1-\pi\rho_0/g}2\pi\rho_0/g\right)2\pi\rho_0/g + 2\right]$$

and

$$\kappa \approx -\frac{1 - \sqrt{\lambda}\pi/2}{1 + \frac{1}{2}\ln(\lambda/4)}$$

To approximately account for the increase in gap dimensions at the plane surface in the case of rounded corners take

$$\rho'_e = \frac{(b + \rho_0/2) - (a - \rho_0/2)}{\ln\left[(b + \rho_0/2)/(a - \rho_0/2)\right]}$$

so that

$$A_e = \pi\rho_e'^2 \approx (0.6264)\,\pi b^2$$

Note that it is more consistent to also use this parameter in the capacitance formula. However to obtain extremely accurate results we must, in addition, also change the corner rounding geometry to more accurately represent the circular geometry by a very slight reduction in the radius $\rho_0 \to \rho_1$. This is discussed in preceding sections.

The total capacitance is thus

$$C_{tot} = C + \Delta C_{corn} + \Delta C_{coax} + \Delta C_{plastic} \approx 12.9\text{ pF} - 2.7\text{ pF} + 31.02\text{ pF} + 0.83\text{ pF} \approx 42.1\text{ pF}$$

and the effective height to the terminating transmission line is then (using the rounded corner formula)

$$h_e^{trans} \approx A_e/\{(C_{tot})/\varepsilon\} \approx 7.69 \times 10^{-4}\text{ m}$$

If the terminating transmission line has characteristic impedance Z_0 then the voltage wave on the transmission line has amplitude

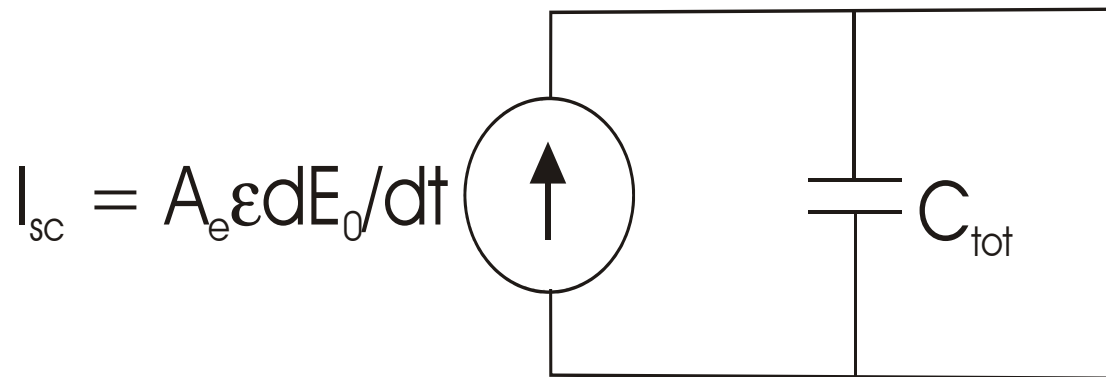$$V(t) = \int_0^t \frac{dV_{oc}}{dt'}(t')\,e^{-(t-t')/\tau}dt'$$

$$I_{sc} = A_e \varepsilon dE_0/dt$$

Figure 10. Norton equivalent circuit for probe.

$$V_{oc} = h_e^{trans} E_0$$

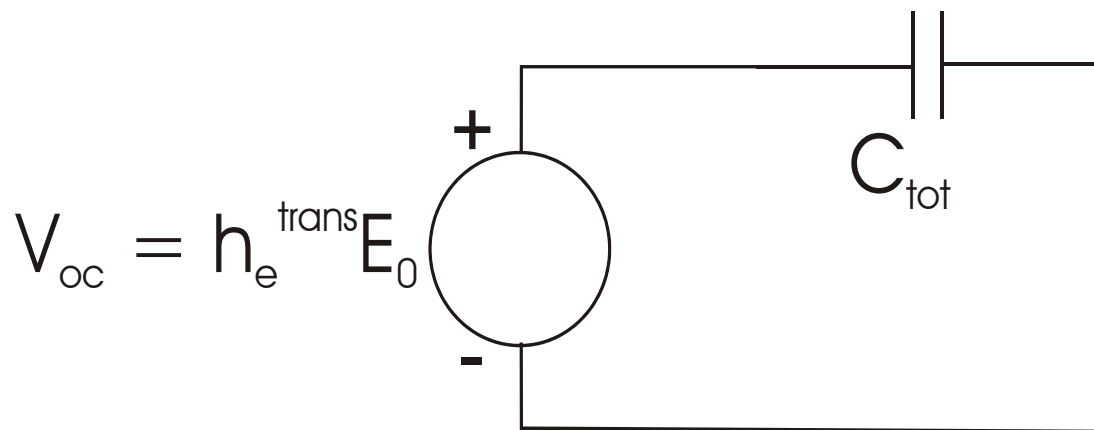Figure 11. Thévenin circuit for probe.

where say $Z_0 \approx 50$ ohms and

$$\tau = Z_0 C_{tot} \approx 2 \text{ ns} + ...$$

The relation between the probe short circuit current, the normal field at the probe E_0, and the current wave on the transmission line $I(t)$ is

$$\int_0^t I_{sc}(t')\,dt' = \varepsilon A_e E_0(t) = \int_0^t I(t')\,dt' + \tau I(t)$$

However when times of interest are long compared to τ the capacitive voltage dominates the circuit and the transmission line voltage and current are found as

$$V = Z_0 I \approx Z_0 I_{sc} = \tau \frac{d}{dt} V_{oc} = Z_0 A_e \varepsilon \frac{d}{dt} E_0 \approx (1.61 \text{ ps-m}) \frac{d}{dt} E_0$$

Since the capacitance is not really needed to find the probe response in this case, given the effective area, the response will be quite stable if the basic geometrical parameters, such as the coaxial radii near the ground plane and flush mounting of the center conductor with respect to the ground plane, are stable.

References

[1] M. E. Morris and T. T. Wu, "Admittance of thin, coaxially-driven infinite monopole antennas," Journal of Electromagnetic Waves and Applications, Vol. 10, No. 5, 1996, pp. 643-692.

[2] D. C. Chang, "Input Admittance and Complete Near-Field Distribution of an Annular Aperture Antenna Driven by a Coaxial Line," IEEE Transactions on Antennas and Propagation, Vol. AP-18, No. 5, Sept. 1970, pp. 610-616.

[3] C. H. Papas, "An Application of Sommerfeld's Complex Order Wave Functions to Antenna Theory," Journal of Math. & Phys., 33, 1954, pp. 269-275.

[4] G. W. C. Kaye and T. H. Laby, **Tables of Physical and Chemical Constants**, Essex: Longman Scientific & Technical, 1986, p. 136.

[5] S. Ramo, J. R. Whinnery, and T. Van Duzer, **Fields and Waves in Communication Electronics**, New York: John Wiley & Sons, 1965, pp. 309-311.

[6] M. Abramowitz and I. a. Stegun (editors), **Handbook of Mathematical Functions**, New York: Dover Pub., Inc., 1972, pp. 79-89.

[7] S.A. Schelkunoff and H.T. Friis, **Antennas Theory and Practice**, New York: John Wiley & Sons, 1952, pp. 553-556.

[8] H. Levine and C. H. Papas, "Theory of the Circular Diffraction Antenna," Journal of Applied Physics, Vol. 22, No. 1, Jan. 1951, pp. 29-43.

[9] M. E. Morris and L.K. Warne, "Accurate Numerical Calculations For Monopole Electric Field Probes," SAND report, to be published.

[10] L.K. Warne and L.I. Basilio, "Formulation for Coaxial Antenna Problem", SAND report, to be published.

[11] W. R. Smythe, **Static and Dynamic Electricity**, New York: Hemisphere Pub. Corp., 1986, pp. 98-100.

[12] G. F. Carrier, M. Krook, and C. E. Pearson, **Functions of a Complex Variable**, Ithaca, New York: Hod Books, 1983, pp. 154-157.

[13] N. Engheta, K. S. H. Lee, and F. C. Yang, "Memo Series On HPM Generic Coupling Memo #9: Umbilical Connector," Dikewood (Division of Kaman Sciences) Internal Report, June 26, 1986.

[14] L. K. Warne and J. R. Barnum, "Simple Approximate Models for Electric and Magnetic Field Derivative Probes," Sandia Laboratories Internal Report, 1996.

[15] N. Marcuvitz, **Waveguide Handbook**, London: Peter Peregrinus Ltd., 1986, pp. 310-312.

Distribution:

1   ITT Industries/AES
    Attn: K. S. H. Lee
    1033 Gayley Avenue
    Suite 215
    Los Angeles, CA 90024

5	MS1152	W. A. Johnson, 01642
1	MS1152	R. E. Jorgenson, 01642
10	MS1152	L. K. Warne, 01642
5	MS1152	L. I. Basilio, 01642
1	MS1152	M. L. Kiefer, 01642
1	MS1152	L. X. Schneider, 01643
5	MS1152	M. E. Morris, 01642
5	MS1152	M. B. Higgins, 01643
1	MS1152	M. Caldwell, 01643
1	MS1152	M. A. Dinallo, 01643
1	MS1194	K. W. Struve, 01644
1	MS1194	M.E. Savage, 01644
1	MS1193	J. E. Maechen, 01645
5	MS1193	J. M.. Lehr, 01645
1	MS0775	J.R. Barnum, 04152
1	MS0405	K. O. Merewether, 12333
1	MS0492	K. C. Chen, 12332
1	MS9018	Central Technical Files, 8945-1
2	MS0899	Technical Library, 09616